Russ. J. Numer. Anal. Math. Modelling, Vol. 27, No. 4, pp. 369–385 (2012)
DOI 10.1515/rnam-2012-0020

Minimal stencil finite volume scheme with the discrete maximum principle

K. LIPNIKOV*, D. SVYATSKIY*, and Yu. VASSILEVSKI†

Abstract — We propose a cell-centered finite volume (FV) scheme with the minimal stencil formed by the closest neighboring cells. The discrete solution satisfies the discrete maximum principle and approximates the exact solution with second-order accuracy. The coefficients in the FV stencil depend on the solution; therefore, the FV scheme is nonlinear. The scheme is applied to a steady state advection-diffusion equation discretized on a general polygonal mesh.

The maximum (or minimum) principle is an important property of solutions of linear and nonlinear partial differential equations (PDEs). Its discrete counterpart is a very desirable property to have in a numerical scheme. Unfortunately, schemes satisfying the discrete maximum principle (DMP) impose severe limitations on mesh regularity [17] and problem coefficients. Violation of the DMP leads to various numerical artifacts, such as a heat flow from a cold material to a hot one, that can be amplified by non-linearity of physics.

In this article, we propose a finite volume (FV) scheme for a steady-state advection-diffusion equation with anisotropic coefficients that satisfies the DMP, works on general polygonal meshes, and has a compact stencil. The price to pay for this flexibility is that the scheme is nonlinear even for linear problems.

The classical two-point FV scheme for diffusion problems defines a flux across a mesh edge as the difference of two concentrations at neighboring cells multiplied by a transmissibility coefficient. It results in a system of algebraic equation with an M-matrix with diagonal dominance in rows, which immediately implies the discrete maximum principle [4, 32]. However, the accuracy of this scheme depends on the mesh geometry, mutual orientation of the mesh edges and principal directions of the diffusion tensor. More precisely, the principal directions have to be orthogonal to the mesh edges, which is clearly an impossible requirement for arbitrary tensors and/or arbitrary polygonal cells. The multi-point flux approximation (MPFA)

*Los Alamos National Laboratory, Los Alamos, NM 87545, U.S.A.

†Institute of Numerical Mathematics, Gubkina str. 8, Moscow 119333, Russia. Corresponding author. E-mail: yuri.vassilevski@gmail.com

This work was carried out under the auspices of the National Nuclear Security Administration of the U.S. Department of Energy at Los Alamos National Laboratory under Contract No. DE-AC52-06NA25396 and the DOE Office of Science Advanced Scientific Computing Research (ASCR) Program in Applied Mathematics. The third author has been partly supported by RFBR grants 11-01-00971, 12-01-00283 and the Federal Program 'Scientific and Pedagogical Stuff of Innovative Russia'.

scheme solves the accuracy problem by using more than two points in the flux stencil [1] and a matrix of transmissibility coefficients. The MPFA scheme provides a second-order accurate approximation of concentrations, but is often only conditionally stable [16] and conditionally monotone [27].

A new research direction pioneered by Le Potier [28] uses a two-point flux stencil with two coefficients that depend on the concentrations in neighboring cells. A few two-point nonlinear FV schemes proposed in the original paper [28] and developed further in a number of papers (see [9,22,23,26,30] and references therein) guarantee the solution positivity on general meshes for general tensor coefficients. These schemes often introduce auxiliary unknowns at the mesh vertices or edges, whose values are interpolated linearly from the concentrations in the neighboring cells. A few interpolation-free schemes were proposed and analyzed in [22, 23] for diffusion and advection-diffusion problems.

The DMP requires a multi-point nonlinear FV scheme. For diffusion problems, such schemes were proposed in [29,31] using again auxiliary unknowns at the mesh vertices. In this paper, we propose an interpolation-free multi-point nonlinear approximation of diffusive fluxes. The resulting scheme has the minimal stencil and reduces to the classical two-point FV scheme on Voronoi or rectangular meshes for scalar (and, in a few cases, diagonal tensor) coefficients.

Analysis of the DMP in [31] uses two facts: the M-matrix property and the diagonal dominance in the rows. Both properties hold true for each iterative approximation of the discrete solution. Our extension of the multi-point nonlinear FV scheme to advection-diffusion problems uses nonlinear upwind slope-limiting techniques [13, 23] which break the diagonal dominance in rows. A different analysis strategy is employed in this paper to prove the DMP, but only for the discrete solution. Numerical experiments indicate that iterative approximations may violate the DMP.

Finally, we mention a few other research directions towards achieving the DMP. A nonlinear stabilized Galerkin approximation for the Laplace operator is considered in [8]; however, its extension to general elliptic equations is not obvious. A nonlinear flux splitting is proposed in [11]. A nonlinear algebraic flux-correction is analyzed in [19]. Different post-processing techniques are employed in [7, 24, 33]. Abundant literature exists for analysis of the DMP for diffusion problems and linear finite elements (see recent papers [6, 10, 12] and references therein). Monotone discretization of advective fluxes is also a well studied subject. We mention only a few techniques, such as nonlinear slope-limiting [13, 20], algebraic flux correction [18], and nonlinear stabilization [15, 25].

The paper outline is as follows. In Section 2, we introduce the advection-diffusion equation and formulate the necessary conditions for the maximum principle. In Section 3, we describe a new nonlinear FV scheme and a nonlinear solver based on the Anderson acceleration. The proof of the discrete maximum principle is in Section 4. Finally, in Section 5, we illustrate the essential properties of our scheme with a few numerical experiments.

1. Steady-state advection–diffusion equation

Let Ω be a two-dimensional polygonal domain with the Lipschitz boundary Γ. The advection-diffusion equation for unknown concentration c with the Dirichlet boundary condition written in a mixed form reads:

$$\begin{aligned} \mathbf{q} = \mathbf{v}c - \mathbb{K}\nabla c, \quad \operatorname{div} \mathbf{q} &= f \qquad \text{in } \Omega \\ c &= g \qquad \text{on } \Gamma. \end{aligned} \tag{1.1}$$

Here $\mathbb{K}(\mathbf{x})$ is a symmetric positive definite discontinuous (possibly anisotropic) diffusion tensor and $\mathbf{v}(\mathbf{x})$ is a continuous (for simplicity) velocity field, $\operatorname{div} \mathbf{v} \geqslant 0$, $f(\mathbf{x})$ is a source term, and $g(\mathbf{x})$ is a given boundary concentration.

The minimum principle states that for $f \geqslant 0$ the concentration $c(\mathbf{x})$ satisfies [21]:

$$\min_{\mathbf{x}\in\bar{\Omega}} c(\mathbf{x}) \geqslant \min\bigl\{0, \min_{\mathbf{x}\in\Gamma} g(\mathbf{x})\bigr\}.$$

The maximum principle is formulated accordingly: for $f \leqslant 0$ the concentration $c(\mathbf{x})$ satisfies:

$$\max_{\mathbf{x}\in\bar{\Omega}} c(\mathbf{x}) \leqslant \max\bigl\{0, \max_{\mathbf{x}\in\Gamma} g(\mathbf{x})\bigr\}.$$

2. Nonlinear FV scheme

Let $\mathscr{T}$ be a conformal polygonal mesh composed of $N_{\mathscr{T}}$ cells T with edges e. The mesh may include non-convex cells. We assume that $\mathscr{T}$ is edge-connected, i.e. it cannot be split into two sub-meshes having no common edges. Using the orientation of the velocity field, we split the boundary Γ into the outflow, Γ_{out}, and inflow, Γ_{in}, parts.

Let $|T|$ denote the area of the cell T and $|e|$ denote the length of the edge e. We denote by $\mathbf{n}_T$ the exterior unit normal vector to ∂T and by $\mathbf{n}_e$ the normal vector to edge e fixed once and for all and such that $|\mathbf{n}_e| = |e|$. On the boundary edge, the vector $\mathbf{n}_e$ is always exterior. The set of boundary edges is denoted by $\mathscr{E}_\Gamma$, and its proper subset of edges belonging to Γ_{in} is denoted by $\mathscr{E}_\Gamma^{\text{in}}$. Let $\mathbf{x}_T$ denote the center of mass of the cell T, $\mathscr{E}_T$ denote the set of edges of T. Finally, let $\mathbf{x}_e$ be the center of edge e. For simplicity, we assume that the diffusion tensor is constant inside each cell; otherwise, we approximate it by a constant tensor $\mathbb{K}_T$.

The FV scheme uses one degree of freedom, C_T, per cell T collocated at $\mathbf{x}_T$. Integrating the mass balance equation (1.1) over T and using the divergence theorem, we obtain:

$$\sum_{e\in\partial T} \sigma_{T,e}\, \mathbf{q}_e \cdot \mathbf{n}_e = \int_T f \,\mathrm{d}x, \qquad \mathbf{q}_e = \frac{1}{|e|}\int_e \mathbf{q}\,\mathrm{d}s \tag{2.1}$$

where $\mathbf{q}_e \cdot \mathbf{n}_e$ is the total flux across the edge e, and $\sigma_{T,e}$ is either 1 or -1 depending on the mutual orientation of normal vectors $\mathbf{n}_e$ and $\mathbf{n}_T$. In derivation of the FV

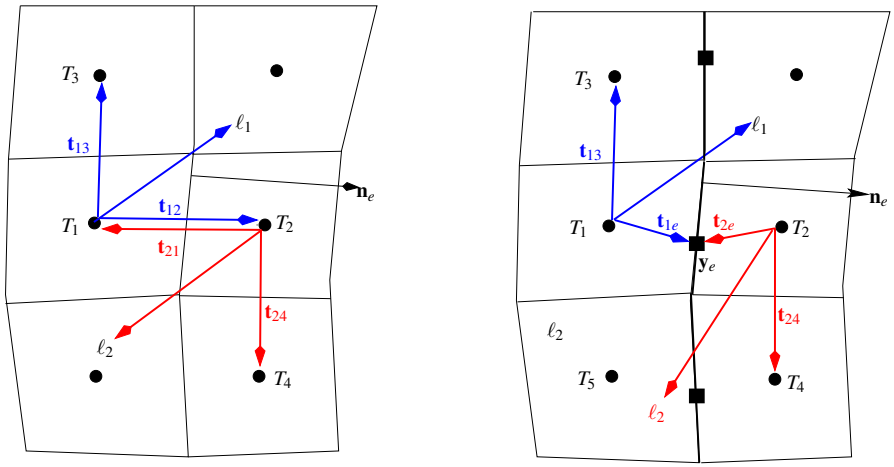

Figure 1. Co-normals ℓ_1 and ℓ_2 and related pairs $\mathbf{t}_{ij}$, $\mathbf{t}_{ik}$ for homogeneous medium (left) and heterogeneous medium (right). The bold edges indicate the material interface. The bold circles indicate the location of collocation points. The bold squares indicate the location of harmonic averaging points.

scheme, we will use the Dirichlet boundary data on edges $e \in \mathcal{E}_\Gamma$, $C_e = \int_e g\,\mathrm{d}s/|e|$, as the known values of the concentration at points $\mathbf{x}_e$.

We present a new approximation for the flux $\mathbf{q}_e \cdot \mathbf{n}_e$ that guarantees the DMP and uses concentrations only in the closest neighboring cells. The latter leads to an algebraic problem with a minimal sparsity structure. A new approximation of the diffusive flux merges the ideas from [5, 22, 29, 31] that assure the DMP with the nonlinear two-point flux FV schemes developed in [9, 23, 26], and the definition of harmonic averaging points proposed in [2]. An approximation of the advective flux uses the second-order upwind FV schemes [3, 13, 23].

2.1. Diffusive flux in homogeneous anisotropic medium

Let us consider a homogeneous medium and connect the collocation point $\mathbf{x}_{T_i}$ of cell T_i with the collocation points $\mathbf{x}_{T_j}$ in its closest neighbors T_j sharing an edge with T_i. Let $\mathbf{t}_{ij} = \mathbf{x}_{T_j} - \mathbf{x}_{T_i}$. We assume that for each edge e of T_i and an associated co-normal vector $\ell_i = \mathbb{K}_{T_i}\mathbf{n}_e$ there exist two vectors $\mathbf{t}_{ij}$ and $\mathbf{t}_{ik}$ (see Fig. 1, left) such that

$$\ell_i = \alpha_{ij}\,\mathbf{t}_{ij} + \alpha_{ik}\,\mathbf{t}_{ik}, \qquad \alpha_{ij} \geqslant 0, \quad \alpha_{ik} \geqslant 0. \tag{2.2}$$

When cell T_i is adjacent to the domain boundary, one can replace T_j and $\mathbf{x}_{T_j}$ in the above formulas with the boundary edge e and its barycenter $\mathbf{x}_e$ [22, 23].

Recalling the definition of the diffusive flux and using finite differences to ap-

proximate directional derivatives, we obtain:

$$\begin{aligned}\mathbf{q}_e^{\mathrm{dif}} \cdot \mathbf{n}_e \equiv -\nabla c \cdot (\mathbb{K}_{T_i} \mathbf{n}_e) &= -\alpha_{ij} \nabla c \cdot \mathbf{t}_{ij} - \alpha_{ik} \nabla c \cdot \mathbf{t}_{ik} \\ &= -\alpha_{ij}(C_{T_j} - C_{T_i}) - \alpha_{ik}(C_{T_k} - C_{T_i}) + O(|e|). \qquad (2.3)\end{aligned}$$

A numerical diffusive flux is obtained by dropping out the approximation term on the right.

Using Fig. 1 (left) and setting $i = 1$, $j = 2$, and $k = 3$ in (2.3), we obtain a numerical diffusive flux, $q_e^{(1)}$, from cell T_1 to cell T_2 through their common edge e. Similarly, setting $i = 2$, $j = 1$, and $k = 4$ in (2.3), we obtain a different numerical flux, $q_e^{(2)}$, in the opposite direction. The final numerical flux is a linear combination of these two fluxes:

$$\begin{aligned}q_e^{\mathrm{dif}} = \mu_1 q_e^{(1)} + \mu_2(-q_e^{(2)}) &= \mu_1(\alpha_{12}(C_{T_1} - C_{T_2}) + \alpha_{13}(C_{T_1} - C_{T_3})) \\ &\quad - \mu_2(\alpha_{21}(C_{T_2} - C_{T_1}) + \alpha_{24}(C_{T_2} - C_{T_4})). \qquad (2.4)\end{aligned}$$

The weights μ_1 and μ_2 are selected to balance the relative contribution of the left and the right fluxes to the final flux:

$$q_e^{(1)} \mu_1 + q_e^{(2)} \mu_2 = 0.$$

The second equation comes from the approximation viewpoint, linear combination (2.4) should be convex:

$$\mu_1 + \mu_2 = 1.$$

If $|q_e^{(1)}| + |q_e^{(2)}| = 0$, the solution of these two equations is not unique and we set $\mu_1 = \mu_2 = 1/2$. Otherwise, we have $|q_e^{(1)}| + |q_e^{(2)}| \neq 0$ and must consider two cases. In the first case $q_e^{(1)} q_e^{(2)} \leqslant 0$ and the solution is

$$\mu_1 = |q_e^{(2)}|/(|q_e^{(1)}| + |q_e^{(2)}|), \quad \mu_2 = |q_e^{(1)}|/(|q_e^{(1)}| + |q_e^{(2)}|).$$

Thus,

$$q_e^{\mathrm{dif}} = \frac{2q_e^{(1)}|q_e^{(2)}|}{|q_e^{(1)}| + |q_e^{(2)}|} = -\frac{2q_e^{(2)}|q_e^{(1)}|}{|q_e^{(1)}| + |q_e^{(2)}|}$$

and the diffusive flux has two equivalent algebraic representations:

$$q_e^{\mathrm{dif}} = 2\mu_1(\alpha_{12}(C_{T_1} - C_{T_2}) + \alpha_{13}(C_{T_1} - C_{T_3})) = A_{12}(C_{T_1} - C_{T_2}) + A_{13}(C_{T_1} - C_{T_3}) \qquad (2.5)$$

and

$$-q_e^{\mathrm{dif}} = 2\mu_2(\alpha_{21}(C_{T_2} - C_{T_1}) + \alpha_{24}(C_{T_2} - C_{T_4})) = A_{21}(C_{T_2} - C_{T_1}) + A_{24}(C_{T_2} - C_{T_4}) \qquad (2.6)$$

with non-negative coefficients A_{12}, A_{13}, A_{21}, and A_{24}. Note that these coefficients depend on the fluxes and hence on the concentrations at neighboring cells. The second case, $q_e^{(1)} q_e^{(2)} > 0$, leads to a potentially degenerate diffusive flux. In order to avoid this degeneracy, the authors in [31] re-group the terms in equation (2.4) as follows:

$$q_e^{\mathrm{dif}} = \mu_1 \bar{q}_e^{(1)} + \mu_2(-\bar{q}_e^{(2)}) + (\mu_1\alpha_{12} + \mu_2\alpha_{21})(C_{T_1} - C_{T_2}) \tag{2.7}$$

where $\bar{q}_e^{(1)} = \alpha_{13}(C_{T_1} - C_{T_3})$, $\bar{q}_e^{(2)} = \alpha_{24}(C_{T_2} - C_{T_4})$. The coefficients μ_1 and μ_2 are computed as before by balancing the modified numerical fluxes:

$$\bar{q}_e^{(1)}\mu_1 + \bar{q}_e^{(2)}\mu_2 = 0$$

and using the convexity condition. Again, if the solution is not unique, we set $\mu_1 = \mu_2 = 1/2$. For the case $\bar{q}_e^{(1)}\bar{q}_e^{(2)} \leqslant 0$, we obtain

$$\begin{aligned} q_e^{\mathrm{dif}} =& 2\mu_1\bar{q}_e^{(1)} + (\alpha_{12} + \mu_2\alpha_{21})(C_{T_1} - C_{T_2}) \\ =& A_{13}(C_{T_1} - C_{T_3}) + A_{12}(C_{T_1} - C_{T_2}) \\ =& -2\mu_2\bar{q}_e^{(2)} - (\alpha_{12} + \mu_2\alpha_{21})(C_{T_2} - C_{T_1}) \\ =& -A_{24}(C_{T_2} - C_{T_4}) - A_{21}(C_{T_2} - C_{T_1}) \end{aligned} \tag{2.8}$$

where $A_{12} = A_{21} = \mu_1\alpha_{12} + \mu_2\alpha_{21}$. For the case $\bar{q}_e^{(1)}\bar{q}_e^{(2)} > 0$, we obtain

$$q_e^{\mathrm{dif}} = (\mu_1\alpha_{12} + \mu_2\alpha_{21})(C_{T_1} - C_{T_2}) = A_{12}(C_{T_1} - C_{T_2}). \tag{2.9}$$

The coefficients A_{12}, A_{13}, and A_{24} in (2.8), (2.9) are non-negative by construction.

Note briefly that calculating A_{ij}, inserting the diffusive fluxes in the mass balance equation, and neglecting other terms, we get an algebraic problem with an M-matrix, which has a diagonal dominance in its rows. The stencil of this matrix is smaller than that in [31]. For a logically square mesh, the proposed FV scheme results in a five-point stencil contrary to a nine-point stencil in [31].

2.2. Diffusive flux in heterogeneous anisotropic medium

Let us consider a heterogeneous medium. Without loss of generality, it is sufficient to describe the approximation of the diffusive flux in the case of two materials, as illustrated in Fig. 1 (right).

Let an interface edge e be shared by cells T_1 and T_2. We denote the line containing e by p_e and consider a continuous piecewise linear function $\mathscr{R}(\mathbf{x})$ such that

$$\mathscr{R}(\mathbf{x}_{T_1}) = C_{T_1}, \quad \mathscr{R}(\mathbf{x}_{T_2}) = C_{T_2}$$

and the diffusive flux is continuous:

$$\mathbb{K}_{T_1}\nabla\mathscr{R}(\mathbf{x})\cdot\mathbf{n}_e = \mathbb{K}_{T_2}\nabla\mathscr{R}(\mathbf{x})\cdot\mathbf{n}_e.$$

Then, there exist a *harmonic averaging point* $\mathbf{y}_e \in p_e$ and a coefficient α_e independent of $\mathscr{R}$ such that [2]:

$$C_e \equiv \mathscr{R}(\mathbf{y}_e) = \alpha_e C_{T_1} + (1-\alpha_e) C_{T_2}, \quad 0 \leqslant \alpha_e \leqslant 1 \tag{2.10}$$

where

$$\alpha_e = \frac{d_{2,e}\mathbf{n}_e \cdot (\mathbb{K}_{T_1}\mathbf{n}_e)}{d_{2,e}\mathbf{n}_e \cdot (\mathbb{K}_{T_1}\mathbf{n}_e) + d_{1,e}\mathbf{n}_e \cdot (\mathbb{K}_{T_2}\mathbf{n}_e)}$$

and $d_{i,e}$ is the distance from point $\mathbf{x}_{T_i}$ to line p_e.

The method described in the previous section can be adjusted to discontinuous tensors by using harmonic averaging points. We note that approximation of the directional derivative $\nabla c \cdot \mathbf{t}_{ij}$ is accurate only inside each material. This limits significantly the number of admissible directions $\mathbf{t}_{ij}$ to the point that expansion (2.2) does not exist. The additional vectors $\mathbf{t}_{ie}$ from collocation points $\mathbf{x}_{T_i}$ and $\mathbf{x}_{T_j}$ to the harmonic point $\mathbf{y}_e$ can be used to find the expansion.

Figure 1(right) illustrates the case when the harmonic averaging point $\mathbf{y}_e$ is inside the edge e so that the vectors $\mathbf{t}_{1e}$ and $\mathbf{t}_{2e}$ do not cross the material interface and the respective directional derivatives are accurate. The formula for the resulting final diffusive flux $\mathbf{q}_e^{\mathrm{dif}}$ involves both C_{T_i} and C_e. The latter can be eliminated using the convex combination (2.10) without increasing the stencil size and preserving the DMP. For example, formula (2.5) is modified as follows:

$$q_e^{\mathrm{dif}} = A_{12}(C_{T_1} - C_e) + A_{13}(C_{T_1} - C_{T_3}) = A_{12}(1-\alpha_e)(C_{T_1} - C_{T_2}) + A_{13}(C_{T_1} - C_{T_3}). \tag{2.11}$$

The other formulas are modified similarly.

It is pertinent to note that the presented scheme can be used even when $\mathbf{y}_e \notin e$. Indeed, consider a piecewise linear function $\mathscr{R}(\mathbf{x})$ that provides the best local approximation of the continuous solution $c(\mathbf{x})$. Then, the error associated with this approximation will be the dominant error in the numerical diffusive flux. The actual geometric location of the point $\mathbf{y}_e$ becomes irrelevant.

2.3. Advective flux

To approximate the total advective flux across the edge e,

$$\mathbf{q}_e^{\mathrm{adv}} = \int_e c\mathbf{v}\,\mathrm{d}x$$

we use the second-order upwind approximation. Let us define a discontinuous piecewise linear function $\mathscr{R}(\mathbf{x})$ (different from the one introduced above) and denote its restriction to cell T as $\mathscr{R}_T(\mathbf{x})$. Let the edge e be shared by cells T_i and T_j and the vector $\mathbf{n}_e$ be exterior to T_i. Then, we define

$$\mathbf{q}_e^{\mathrm{adv}} \cdot \mathbf{n}_e = v_e^+ \mathscr{R}_{T_i}(\mathbf{x}_e) + v_e^- \mathscr{R}_{T_j}(\mathbf{x}_e) \tag{2.12}$$

where

$$v_e^+ = \frac{1}{2}(v_e + |v_e|), \qquad v_e^- = \frac{1}{2}(v_e - |v_e|), \qquad v_e = \frac{1}{|e|}\int_e \mathbf{v}\cdot\mathbf{n}_e \,\mathrm{d}x. \tag{2.13}$$

The linear reconstruction has to be limited to get a monotone scheme. Following [23], we use a tensorial limiter:

$$\mathscr{R}_T(\mathbf{x}) = C_T + \mathscr{L}_T(\mathbf{g}_T)\cdot(\mathbf{x}-\mathbf{x}_T) \qquad \forall \mathbf{x}\in T \tag{2.14}$$

where $\mathbf{g}_T$ is the reconstructed gradient and $\mathscr{L}_T$ is a limiting 2×2 matrix. This reconstruction preserves the mean value of the concentration for any choice of $\mathscr{L}_T$. The admissible gradient $\tilde{\mathbf{g}}_T = \mathscr{L}_T(\mathbf{g}_T)$ must result in a linear reconstruction that is bounded at the neighboring collocation points $\mathbf{x}_k$, which are either the barycenters of the closest neighboring cells T', or the centers of boundary edges $e' \in \mathscr{E}_\Gamma \cap \mathscr{E}_T$:

$$\min\{C_{T'}; C_{e'}\} \leqslant C_T + \tilde{\mathbf{g}}_T\cdot(\mathbf{x}_k - \mathbf{x}_T) \leqslant \max\{C_{T'}; C_{e'}\}. \tag{2.15}$$

Due to (2.15), we get that $\tilde{\mathbf{g}}_T \equiv 0$ in local minima and maxima. The derivation of the limiting matrix is described in detail in [23] and will not be repeated here.

Remark 2.1. According to the numerical evidence, for a singularly perturbed advection-diffusion equation, conditions (2.15) should be weakened [23]. More precisely, the upper bound should involve only inflow boundary edges $e'' \in \mathscr{E}_\Gamma^{\mathrm{in}} \cap \mathscr{E}_T$:

$$\min\{C_{T'}; C_{e'}\} \leqslant C_T + \tilde{\mathbf{g}}_T\cdot(\mathbf{x}_k - \mathbf{x}_T) \leqslant \max\{C_{T'}; C_{e''}\}. \tag{2.16}$$

Remark 2.2. The linear first-order upwind approximation is obtained by setting $\mathscr{R}_T(\mathbf{x}) = C_T$ so that

$$\mathbf{q}_e^{\mathrm{adv}}\cdot\mathbf{n}_e = v_e^+ C_{T_i} + v_e^- C_{T_j}. \tag{2.17}$$

2.4. Anderson acceleration

Let $\mathbf{C}$ be the vector of all cell-centered unknowns. Replacing the fluxes in equations (2.1) by their numerical approximations, we obtain a system of nonlinear equations

$$\mathbf{M}(\mathbf{C})\,\mathbf{C} = \mathbf{F}(\mathbf{C}), \qquad \mathbf{M}(\mathbf{C}) = \mathbf{M}_{\mathrm{dif}}(\mathbf{C}) + \mathbf{M}_{\mathrm{adv}}(\mathbf{C}) \tag{2.18}$$

with a square matrix $\mathbf{M}$ and a right-hand side vector $\mathbf{F}$ whose entries are defined by formulas (2.1), (2.5), (2.6), (2.8), (2.9), (2.11), and (2.12). Algebraically, contributions from the diffusive and advective fluxes lead to summation of two M-matrices as shown in (2.18). The first (diffusion) matrix has diagonal dominance in rows, the second (advection) matrix – in columns (see [23]). Since this sum does not always preserve the diagonal dominance in rows, a proof of the DMP for the solution of (2.18) becomes nontrivial.

The efficient solution of this system is crucial for practical usage of the proposed FV scheme. We recommend the Anderson acceleration technique (see Algorithm 2.1 below), which does not require computation of the Jacobian and relies on the approximate solution of linearized systems. Contrary to the Picard method, the Anderson acceleration method does not guarantee the DMP for intermediate iterative approximations $\mathbf{C}^{k+1}$ neither for diffusion, nor for advection–diffusion problems. The DMP holds only for the converged solution.

Algorithm 2.1. Anderson acceleration.

1: Choose $\mathbf{C}^0$ and a fixed integer number m.
2: Apply m Picard iterations $\mathbf{C}^k = \mathbf{M}(\mathbf{C}^{k-1})^{-1}\mathbf{F}(\mathbf{C}^{k-1})$ and set $\widetilde{\mathbf{C}}^k = \mathbf{C}^k$, $\delta\mathbf{C}^k = \widetilde{\mathbf{C}}^k - \widetilde{\mathbf{C}}^{k-1}$, $k = 1,\dots,m$.
3: **for** $k = m,\dots$ **do**
4: Determine weights $\alpha_1,\dots,\alpha_m$ by solving the constrained minimization problem

$$\min_{\sum_{i=1}^m \alpha_i = 1} \|\sum_{i=1}^{m} \alpha_i \delta\mathbf{C}^{k-m+i}\|. \tag{2.19}$$

5: Set new iterate:

$$\mathbf{C}^{k+1} = \sum_{i=1}^{m} \alpha_i \widetilde{\mathbf{C}}^{k-m+i}. \tag{2.20}$$

6: Check the convergence criterion for the nonlinear residual.
7: Compute $\widetilde{\mathbf{C}}^{k+1} = \mathbf{M}(\mathbf{C}^{k+1})^{-1}\mathbf{F}(\mathbf{C}^{k+1})$ and set $\delta\mathbf{C}^{k+1} = \widetilde{\mathbf{C}}^{k+1} - \mathbf{C}^k$.
8: **end for**

3. Analysis of the discrete maximum principle

For a pure diffusion equation, the DMP for both the solution of (2.18) and each Picard iterate $\mathbf{C}^k = \mathbf{M}(\mathbf{C}^{k-1})^{-1}\mathbf{F}(\mathbf{C}^{k-1})$ follows from the algebraic result in [4, 32]. In all our experiments the matrix $\mathbf{M}_{\text{dif}}(\mathbf{C}^{k-1})$ have been irreducible, the result which is expected for a diffusion problem.

For an advection-diffusion equation with the first-order upwind approximation of advective fluxes (2.17), the matrix $\mathbf{M}_{\text{adv}}$ has a diagonal dominance in its rows. In order to show this, we consider any cell T such that $\mathscr{E}_T \cap \mathscr{E}_\Gamma^{\text{in}} = \varnothing$ and the corresponding row i in the matrix $\mathbf{M}_{\text{adv}}$ with entries m_{ij}. The definitions of the matrix (2.1), the discrete advective flux (2.17), (2.13), and the assumption $\operatorname{div}\mathbf{v} \geqslant 0$, imply:

$$\sum_j m_{ij} = \sum_{e\in\mathscr{E}_T} v_e^+ \cdot 1 + v_e^- \cdot 1 = \sum_{e\in\mathscr{E}_T} v_e = \int_T \operatorname{div}\mathbf{v}\,\mathrm{d}x \geqslant 0.$$

Considering any cell such that $\mathscr{E}_T \cap \mathscr{E}_\Gamma^{\rm in} \neq \varnothing$, we obtain:

$$\sum_j m_{ij} = \sum_{e\in\mathscr{E}_T\setminus\mathscr{E}_\Gamma^{\rm in}} v_e^+ \cdot 1 + v_e^- \cdot 1 = \sum_{e\in\mathscr{E}_T} v_e^+ + v_e^- - \sum_{e\in\mathscr{E}_T\cap\mathscr{E}_\Gamma^{\rm in}} v_e^-$$
$$= \int_T {\rm div}\mathbf{v}\,{\rm d}x - \sum_{e\in\mathscr{E}_T\cap\mathscr{E}_\Gamma^{\rm in}} v_e^- \geqslant \int_T {\rm div}\mathbf{v}\,{\rm d}x \geqslant 0,$$

since $v_e^- \leqslant 0$. Therefore, due to the diagonal dominance in rows of $\mathbf{M}(C^{k-1}) = \mathbf{M}_{\rm dif}(C^{k-1}) + \mathbf{M}_{\rm adv}$, the same algebraic result [4, 32] can be applied to prove the DMP for both the solution of (2.18) and each Picard iterate.

For the second-order upwind approximation (2.12), the proof of the DMP for solution of (2.18) uses ellipticity ($\mathbb{K}(\mathbf{x}) > 0$, ${\rm div}\mathbf{v} \geqslant 0$) of the continuous operator and the special multi-point form of the diffusive flux.

Theorem 3.1 (Minimum principle). *Let a solution* $\mathbf{C}$ *to* (2.18) *exist,* $f \geqslant 0$, ${\rm div}\mathbf{v} \geqslant 0$, *and* $\mathbf{M}_{\rm dif}(\mathbf{C})$ *be an irreducible matrix. Then*

$$\min_{T\in\mathscr{T}} C_T \geqslant C_{\min} \equiv \min\left\{0; \min_{e\in\mathscr{E}_\Gamma} C_e\right\}.$$

Proof. The proof is by a contradiction. Let us consider the cell T with the smallest concentration C_T and assume that $C_T < C_{\min}$. Without lose of generality, we assume that vectors $\mathbf{n}_e$, $e \in \mathscr{E}_T$, are exterior to T. Let $T = T_1$, while T' and T'' stand for T_2 and T_3, respectively, in the diffusive flux formulas, and T_e' stand for the cell sharing the edge e with T. Since C_T is the global minimum, $\tilde{\mathbf{g}}_T = 0$ and $\mathscr{R}_T \equiv C_T$ due to (2.15). The definition of advective fluxes gives

$$\sum_{e\in\mathscr{E}_T} \mathbf{q}_e^{\rm adv}\cdot\mathbf{n}_e = \sum_{e\in\mathscr{E}_T\setminus\mathscr{E}_\Gamma^{\rm in}} \left(v_e^+ C_T + v_e^- \mathscr{R}_{T_e'}(\mathbf{x}_e)\right) + \sum_{e\in\mathscr{E}_T\cap\mathscr{E}_\Gamma^{\rm in}} v_e^- C_e.$$

Since C_T is the local minimum, it holds $\mathscr{R}_{T_e'}(\mathbf{x}_e) \geqslant C_T$ and $C_e > C_T$. Using that $v_e^- = v_e$ on the inflow edges, $v_e = v_e^+ + v_e^-$, the divergence theorem, $v_e^- \leqslant 0$, and the assumption, we obtain

$$\sum_{e\in\mathscr{E}_T} \mathbf{q}_e^{\rm adv}\cdot\mathbf{n}_e \leqslant \sum_{e\in\mathscr{E}_T\setminus\mathscr{E}_\Gamma^{\rm in}} (v_e^+ + v_e^-) C_T + \sum_{e\in\mathscr{E}_T\cap\mathscr{E}_\Gamma^{\rm in}} v_e^- C_T = C_T \sum_{e\in\mathscr{E}_T} v_e = C_T \int_T {\rm div}\mathbf{v}\,{\rm d}x \leqslant 0.$$

A similar argument can be used for diffusive fluxes. Since C_T is the local minimum, each of the three possible discrete diffusive fluxes is negative. For fluxes (2.5), (2.8), we obtain

$$\mathbf{q}_e^{\rm dif}\cdot\mathbf{n}_e = A_{12}(C_T - C_{T'}) + A_{13}(C_T - C_{T''}) \leqslant 0$$

due to non-negativity of A_{12} and A_{13}. Similarly, for fluxes (2.9) and (2.11), we get

$$\mathbf{q}_e^{\rm dif}\cdot\mathbf{n}_e = A_{12}(C_T - C_{T'}) \leqslant 0$$

and

$$\mathbf{q}_e^{\mathrm{dif}} \cdot \mathbf{n}_e = A_{12}(1-\alpha_e)(C_T - C_{T'}) + A_{13}(C_T - C_{T''}) \leqslant 0.$$

The mass balance equation (2.1),

$$\int_T f \,\mathrm{d}x - \sum_{e \in \mathscr{E}_T} \mathbf{q}_e^{\mathrm{dif}} \cdot \mathbf{n}_e - \sum_{e \in \mathscr{E}_T} \mathbf{q}_e^{\mathrm{dif}} \cdot \mathbf{n}_e = 0 \tag{3.1}$$

implies that all terms are non-negative and must be equal to zero. Therefore, $C_{T'_e} = C_T$ for all neighboring cells T'_e having a non-zero matrix connection with T. The assumption of the matrix irreducibility implies that $\mathbf{C}$ is a constant vector. Finally, considering a cell T with edge $e \in \mathscr{E}_\Gamma$, we obtain that $C_T = C_e$, which contradicts to our assumption and proves the assertion of the theorem.

Theorem 3.2 (Maximum principle). *Let a solution* $\mathbf{C}$ *to (*2.18*) exist,* $f \leqslant 0$*,* $\operatorname{div} \mathbf{v} \geqslant 0$*, and* $\mathbf{M}_{\mathrm{dif}}(\mathbf{C})$ *be an irreducible matrix. Then*

$$\max_{T \in \mathscr{T}} C_T \leqslant C_{\max} \equiv \max \left\{ 0; \max_{e \in \mathscr{E}_\Gamma} C_e \right\}.$$

The proof is similar to that of Theorem 3.1.

4. Numerical experiments

We verify the convergence and monotonicity properties of the proposed nonlinear FV scheme with a few numerical experiments.

4.1. Convergence analysis

The convergence analysis is performed on a sequence of randomly distorted quadrilateral meshes. These meshes are obtained by perturbation of uniform square meshes with the mesh size h. Each internal node (x,y) is relocated to a new position $(\tilde{x},\tilde{y})$ as follows:

$$\tilde{x} := x + \gamma \xi_x h, \qquad \tilde{y} := y + \gamma \xi_y h \tag{4.1}$$

where ξ_x and ξ_y are random variables with values between -0.5 and 0.5 and $\gamma \in [0,1]$ is the degree of distortion. We set $\gamma = 0.6$ to avoid mesh tangling. It is pertinent to emphasize that the distortion is performed at each refinement level. A distorted mesh looks like the mesh shown in Fig. 2 (center).

Let us define the following mesh-dependent norms for a vector $\mathbf{C}$ of cell-based concentrations and a vector $\mathbf{q}$ of edge-based fluxes:

$$|||\mathbf{C}|||^2 = \sum_{T \in \mathscr{T}} |T|\,|C_T|^2, \qquad |||\mathbf{q}|||^2 = \sum_{e \in \mathscr{E}_I \cup \mathscr{E}_B} |S_e|\,|\mathbf{q}_e \cdot \mathbf{n}_e|^2$$

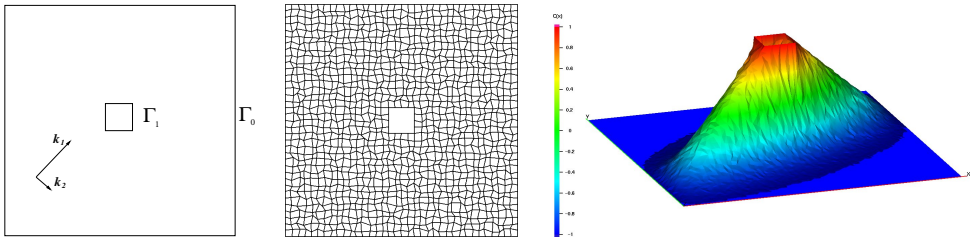

Figure 2. Left: computational domain for the anisotropic diffusion problem. Center: distorted quadrilateral mesh. Right: profile of the numerical solution.

where $|S_e|$ is a representative area for the edge e. More precisely, $|S_e|$ is the arithmetic average of the areas of the mesh cells sharing the edge e. Let $\mathbf{C}^{\rm ex}$ and $\mathbf{q}^{\rm ex}$ be the vectors of exact concentrations and fluxes. We define the following relative errors:

$$\varepsilon_2^c = \frac{|||\mathbf{C}^{\rm ex} - \mathbf{C}|||}{|||\mathbf{C}^{\rm ex}|||}, \qquad \varepsilon_2^q = \frac{|||\mathbf{q}^{\rm ex} - \mathbf{q}|||}{|||\mathbf{q}^{\rm ex}|||}.$$

The nonlinear iterations are terminated when the initial residual norm is reduced 10^8 times.

In the first experiment, we consider an advection-diffusion problem in $\Omega = [0,1]^2$ with a smooth solution. The anisotropic discontinuous diffusion tensor is given by:

$$\mathbb{K} = \begin{cases} \mathbb{K}^1 = 1, & x < 1/2 \\ \mathbb{K}^{(2)} = R(-\theta) \begin{bmatrix} 10^2 & 0 \\ 0 & 1 \end{bmatrix} R(\theta), & x \geqslant 1/2 \end{cases}$$

where $R(\theta)$ is the clock-wise rotation matrix and $\theta = \pi/6$. We set a constant velocity vector, $\mathbf{v} = (3,-2)^T$, and choose the following exact solution:

$$c(x,y) = \begin{cases} 1 - 2y^2 + 4xy + 2y + 6x, & x < 1/2 \\ b_2 y^2 + c_2 xy + d_2 x + e_2 y + f_2, & x \geqslant 1/2 \end{cases} \tag{4.2}$$

where

$$b_2 = -2, \quad c_2 = \frac{4\mathbb{K}_{11}^{(2)} - 2\mathbb{K}_{12}^{(2)} - 2}{\mathbb{K}_{11}^{(2)}}, \quad d_2 = \frac{4(\mathbb{K}_{12}^{(2)} + 1)}{\mathbb{K}_{11}^{(2)}}$$

$$e_2 = \frac{4\mathbb{K}_{11}^{(2)} - 2\mathbb{K}_{12}^{(2)} - 2}{\mathbb{K}_{11}^{(2)}}, \quad f_2 = \frac{4\mathbb{K}_{11}^{(2)} + 2\mathbb{K}_{12}^{(2)} - 3}{\mathbb{K}_{11}^{(2)}}.$$

The coefficients b_2, c_2, d_2, e_2, f_2 are defined to provide the continuity of the solution and its flux.

Table 1.
The convergence results for the problem with the smooth solution (4.2).

h	$\varepsilon_2^C c$	ε_2^q
1/16	1.38e−03	4.13e−02
1/32	3.86e−04	1.56e−02
1/64	1.05e−04	6.01e−03
1/128	2.69e−05	2.47e−03
1/256	6.40e−06	1.11e−03
rate	1.93	1.31

The convergence results presented in Table 1 indicate that the FV scheme is second-order accurate. A super linear convergence of fluxes has been also observed in other experiments and requires further analysis.

4.2. Discrete maximum principle for anisotropic diffusion problem

In the second experiment, we demonstrate the DMP property of the proposed FV scheme for a highly anisotropic diffusion problem. The problem is defined in a unit square with a square hole in the center, $\Omega = (0,1)^2/[4/9,5/9]^2$, and the diffusion tensor is homogeneous but anisotropic:

$$\mathbb{K} = R(-\theta)\begin{bmatrix} 1 & 0 \\ 0 & 10^{-3} \end{bmatrix} R(\theta), \qquad \theta = 67.5^\circ.$$

The domain boundary consists of two disjoint parts: internal Γ_1 and external Γ_0. We impose the Dirichlet boundary conditions as $c = 1$ on Γ_1 and $c = -1$ on Γ_0. A scheme of the computational domain Ω with the primary directions of the diffusion tensor is shown in Fig.2 (left). Finally, we set $f = 0$, so that according to the maximum and minimum principles, the solution should vary between -1 and 1. The numerical solution computed on a coarse distorted quadrilateral mesh is shown in Fig.2 (right). This solution satisfies the DMP.

4.3. Discrete maximum principle for advection dominated problem

In the third set of numerical experiments, we demonstrate the monotone property of the FV scheme for an advection-diffusion problem. These numerical results illustrate the conclusions derived in Theorems 3.1 and 3.2.

Let us consider a problem with discontinuous Dirichlet boundary data. The discontinuity produces an internal shock in the solution, in addition to the exponential boundary layers. This is a popular test case for discretization schemes designed for advection-dominated problems (see [14, 15]). Following [15], we set

$$\mathbf{v} = \left(\cos\frac{\pi}{3}, -\sin\frac{\pi}{3}\right), \qquad \mathbb{K} = \nu\mathbb{I}, \qquad \nu = 10^{-8}.$$

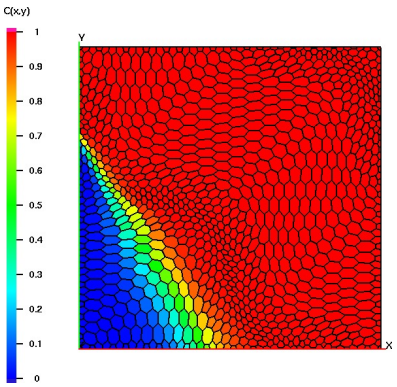

Figure 3. The DMP test for advection–diffusion problem: the numerical solution varies between 0 and 1.

The Dirichlet boundary conditions are as follows:

$$c(x,y) = \begin{cases} 0 & \text{if } x = 1 \text{ or } y \leqslant 0.7 \\ 1 & \text{otherwise.} \end{cases}$$

The exact solution has a boundary layer next to two boundary lines $y = 0$ and $x = 1$. It also has an internal layer along the velocity streamline passing through point $(0, 0.7)$.

The problem is discretized on the unstructured polygonal mesh shown in Fig. 3 with 4096 cells and the effective mesh parameter $h = 1/64$. The mesh Péclet number is $\mathrm{Pe} = 781\,250$.

In order to measure the quality of the numerical solution, the authors of [15] have proposed several estimates which quantify the numerical solution oscillations and smearing effects caused by the discretization scheme. Let $\Omega_1 = \{(x,y) \in \Omega : x \leqslant 1/2,\ y \geqslant 0.1\}$, $\Omega_2 = \{(x,y) \in \Omega : x \geqslant 0.7\}$, and Ω_3 denote a cell strip in the vicinity of the line $y = 0.25$,

$$\Omega_3 = \{T \in \mathscr{T} : \mathbf{x}_T = (x_T, y_T),\ |y_T - 0.25| \leqslant |T|^{1/2}\}.$$

First, we define two estimates which characterize the undershoots and overshoots in Ω_1, respectively:

$$\mathrm{osc}_{\mathrm{int}}^{\min} \equiv \Big(\sum_{\mathbf{x}_T \in \Omega_1} (\min\{0, C_T\})^2 \Big)^{1/2} \tag{4.3}$$

$$\mathrm{osc}_{\mathrm{int}}^{\max} \equiv \Big(\sum_{\mathbf{x}_T \in \Omega_1} (\max\{0, C_T - 1\})^2 \Big)^{1/2}. \tag{4.4}$$

Second, we define an estimate which quantifies the oscillations near the boundary layer in Ω_2:

$$\mathrm{osc}_{\mathrm{exp}} \equiv \Big(\sum_{\mathbf{x}_T \in \Omega_2} (\max\{0, C_T - 1\})^2 \Big)^{1/2}. \tag{4.5}$$

Table 2.
The quality of numerical solutions in two nonlinear FV schemes.

	Positivity preserving FV scheme	FV scheme with DMP
$\text{osc}_{\text{int}}^{\min}$	0	0
$\text{osc}_{\text{int}}^{\max}$	6.96e−08	1.91e−15
osc_{exp}	1.84e−13	2.99e−15
$\text{smear}_{\text{int}}$	1.13e−01	1.13e−01
$\text{smear}_{\text{exp}}$	8.36e−05	7.05e−05

Third, we define two estimates which measure the thickness of the boundary layer and the internal shock, respectively:

$$\text{smear}_{\text{exp}} \equiv \Big(\sum_{\mathbf{x}_T \in \Omega_2} (\min\{0, C_T - 1\})^2 \Big)^{1/2} \tag{4.6}$$

$$\text{smear}_{\text{int}} \equiv x_2 - x_1 \tag{4.7}$$

where

$$x_1 = \min_{\mathbf{x}_T \in \Omega_3, C_T \geqslant 0.1} x_T, \qquad x_2 = \max_{\mathbf{x}_T \in \Omega_3, C_T \leqslant 0.9} x_T.$$

For the continuous solution these estimates depend on the diffusion process only, so they are much smaller than the considered mesh size. For the numerical solution, the small values of estimates (4.3)–(4.7) characterize the almost non-oscillatory and almost non-diffusive discrete solution.

The results obtained by the nonlinear FV method are shown in Table 2. They are competitive with the best results presented in review [15]. We also compare the new scheme to the nonlinear positivity preserving the FV scheme in [23]. The new scheme has about the same smearing properties, but has no overshoots up to the numerical precision.

Conclusion

We have proposed a new nonlinear FV scheme for advection–diffusion equations. The scheme satisfies the discrete maximum principle and has a compact stencil. It reduces to the classical five-point FV scheme stencil on square meshes for diffusion equations with diagonal diffusion tensors. The scheme is second-order accurate for concentrations and at least first-order accurate for fluxes. We have proved the DMP for this scheme and have demonstrated the properties of our scheme with a few numerical experiments.

References

1. I. Aavatsmark, G. Eigestad, B. Mallison, and J. Nordbotten. A compact multipoint flux approximation method with improved robustness. *Numer. Meth. Partial Diff. Equ.* (2008) **24**, No. 5, 1329–1360.

2. L. Agelas, R. Eymard, and R. Herbin. A nine-point finite volume scheme for the simulation of diffusion in heterogeneous media. *C. R. Acad. Sci. Paris, Ser. I* (2009) **347**, 673–676.

3. T.J. Barth and D.C. Jespersen. The design and application of upwind schemes on unstructured meshes. *AIAA Paper 89-0366*, 1989.

4. A. Berman and R. J. Plemmons. *Nonnegative Matrices in the Mathematical Sciences*. Academic Press [Harcourt Brace Jovanovich Publishers], New York, 1979.

5. E. Bertolazzi and G. Manzini. A second-order maximum principle preserving finite volume method for steady convection–diffusion problems. *SIAM J. Numer. Anal.* (2005) **43**, No. 5, 2172–2199.

6. J. H. Brandts, S. Korotov, and M. Krizek. The discrete maximum principle for linear simplicial finite element approximations of a reaction-diffusion problem. *Linear Algebra Appl.* (2009) **429**, No. 10, 2344–2357.

7. O. Burdakov, I. Kapyrin, and Yu. Vassilevski. Monotonicity recovering and accuracy preserving optimization methods for postprocessing finite element solutions. *J. Comp. Phys.* (2012) **231**, 3126–3142.

8. E. Burman and A. Ern. Discrete maximum principle for Galerkin approximations of the Laplace operator on arbitrary meshes. *C. R. Math. Acad. Sci. Paris* (2004) **338**, Nj. 8, 641–646.

9. A. Danilov and Y. Vassilevski. A monotone nonlinear finite volume method for diffusion equations on conformal polyhedral meshes. *Russ. J. Numer. Anal. Math. Modelling* (2009) **24**, No. 3, 207–227.

10. A. Draganescu, T. F. Dupont, and L. R. Scott. Failure of the discrete maximum principle for an elliptic finite element problem. *Math. Comp.* (2004) **74**, No. 249, 1–23.

11. M.G. Edwards and M. Pal. Nonlinear flux-splitting schemes with imposed discrete maximum principle for elliptic equations with highly anisotropic coefficients. *Int. J. Numer. Meth. Fluid* (2011) **66**, No. 3, 299–323.

12. I. Farago, R. Horvath, and S. Korotov. Discrete maximum principles for fe solutions of nonstationary diffusion-reaction problems with mixed boundary conditions. *Numer. Meth. Part. Diff. Equ.* (2011) **27**, No. 3, 702–720.

13. M. Hubbard. Multidimensional slope limiters for MUSCL-type finite volume schemes on unstructured grids. *J. Comp. Phys.* (1999) **155**, No. 1, 54–74.

14. T.J.R. Hughes, M. Mallet, and A. Mizukami. A new finite element formulation for computational fluid dynamics. II. Beyond SUPG. *Comp. Meth. Appl. Mech. Engrg.* (1986) **54**, No. 3, 341–55.

15. V. John and P. Knobloch. On spurious oscillations at layers diminishing (SOLD) methods for convection-diffusion equations: Part I - a review. *Comp. Meth. Appl. Mech. Engrg.*, (2007) **196**, No. 17–20, 2197–2215.

16. R. A. Klause and R. Winther. Convergence of multipoint flux approximations on quadrilateral grids. *Numer. Meth. Part. Diff. Equ.* (2006) **22**, 1438–1454.

17. S. Korotov, M. Křížek, and P. Neittaanmäki. Weakened acute type condition for tetrahedral triangulations and the discrete maximum principle. *Math. Comp.* (2001) **70**, No. 233, 107–119.

18. D. Kuzmin and M. Moller. Algebraic flux correction I. scalar conservation laws. (Eds. D. Kuzmin, R. Lohner, and S. Turek) *Flux-Corrected Transport: Principles, Algorithms, And Applications*, pp. 155–206. Springer-Verlag Berlin, 2005.

19. D. Kuzmin, M. J. Shashkov, and D. Svyatskiy. A constrained finite element method satisfying the discrete maximum principle for anisotropic diffusion problems. *J. Comp. Phys.* (2009) **228**, No. 9, 3448–3463.

20. D. Kuzmin and S. Turek. High-resolution FEM-TVD schemes based on a fully multidimensional

flux limiter. *J. Comp. Phys.* (2004) **198**, No. 1, 31–58.

21. O. A. Ladyzhenskaya and N. N. Uraltseva. *Linear and Quasilinear Elliptic Equations*. Leon Ehrenpreis Academic Press, New York–London, 1968.
22. K. Lipnikov, D. Svyatskiy, and Y. Vassilevski. Interpolation-free monotone finite volume method for diffusion equations on polygonal meshes. *J. Comp. Phys.* (2009) **228**, No. 3, 703–716.
23. K. Lipnikov, D. Svyatskiy, and Y. Vassilevski. A monotone finite volume method for advection–diffusion equations on unstructured polygonal meshes. *J. Comp. Phys.* (2010) **229**, 4017–4032.
24. R. Liska and M. Shashkov. Enforcing the discrete maximum principle for linear finite element solutions of second-order elliptic problems. *Commun. Comp. Phys.* (2008) **3**, No. 4, 852–877.
25. G. Manzini and A. Russo. A finite volume method for advection–diffusion problems in convection–dominated regimes. *Comp. Meth. Appl. Mech. Engrg.* (2008) **197**, No. 13–16, 1242–1261.
26. K. Nikitin and Y. Vassilevski. A monotone nonlinear finite volume method for advection–diffusion equations on unstructured polyhedral meshes in 3D. *Russ. J. Numer. Anal. Math. Modelling* (2010) **25**, No. 4, 335–358.
27. J. M. Nordbotten, I. Aavatsmark, and G. T. Eigestad. Monotonicity of control volume methods. *Numer. Math.* (2007) **106**, No. 2, 255–288.
28. C. Le Potier. Schema volumes finis monotone pour des operateurs de diffusion fortement anisotropes sur des maillages de triangle non structures. *C. R. Math. Acad. Sci. Paris* (2005) **341**, 787–792.
29. C. Le Potier. Finite volume scheme satisfying maximum and minimum principles for anisotropic diffusion operators (Eds. R. Eymard and J.-M. Herard). *Finite Volumes for Complex Applications V*, pp. 103–118, 2008.
30. Z. Sheng and A. Yuan. Monotone finite volume schemes for diffusion equations on polygonal meshes. *J. Comp. Phys.* (2008) **227**, 6288–6312.
31. Z. Sheng and G. Yuan. The finite volume scheme preserving extremum principle for diffusion equations on polygonal meshes. *J. Comp. Phys.* (2011) **230**, No. 7, 2588–2604.
32. G. Stoyan. On maximum principles for monotone matrices. *Linear Algebra and Its Applications* (1986) **78**, 147–161.
33. Y. Yao and G. Yuan. Enforcing positivity with conservation for nine-point scheme of nonlinear diffusion equations. *Comp. Meth. Appl. Math.* (2012), No. 223–224, 161–172.